# MODELING THE EFFECT OF OUT-OF-PLANE FIBER ORIENTATION IN LUMBER SPECIMENS

*Douglas C. Stahl* and *Steven M. Cramer*

Research Assistant and Assistant Professor
Department of Civil and Environmental Engineering
University of Wisconsin–Madison
Madison, WI 53706

and

*Kent McDonald*

Research Wood Scientist
USDA, Forest Service
Forest Products Laboratory[1]
Madison, WI 53705

(Received March 1989)

ABSTRACT

A method is presented to account for the effect of three-dimensional fiber orientations near knots in a two-dimensional lumber tensile strength prediction model. Data we have collected show that grain angles dive from 15 to 90 degrees out of the wide face plane of flat-grained lumber within a region of about one knot radius from the visual edge of a knot. The diving nature of the grain angles is accounted for in a two-dimensional model, called GASPP+, by transforming a three-dimensional material compliance matrix, and extracting the appropriate coefficients for use in a two-dimensional compliance matrix. Failure criteria are modified to reflect the decreased strength associated with nonzero dive angles. These modifications led to accurate tensile behavior predictions, as evidenced by load-displacement plots and ultimate load measurements of lumber specimens. It is shown that consideration of dive angles is important in predicting the tensile strength and failure mode of thin lumber specimens. Lumber specimen thickness and the manner of loading influence the magnitude of the dive effect on strength.

*Keywords:* Fiber orientation, lumber tensile strength, fracture, finite elements.

## INTRODUCTION

To ensure that lumber continues to be a viable option as a structural material, methods must be developed to predict more accurately its behavior, especially its ultimate strength. By eliminating some of the uncertainty in present grading procedures, boards that are predicted to have higher strengths can be assigned those strengths with confidence. Sawn lumber could be used more efficiently; this would open up some applications where sawn lumber is presently not an option because of economic or purely structural reasons.

The behavior of defect-containing sawn lumber is extremely complex even under simple loading conditions. The board with a knot and associated grain deviations is an orthotropic material with variable orientation of orthotropic axes, with material properties that vary with location, with discontinuities and associated stress concentrations, and with the potential for multiple failure modes

[1] The Forest Products Laboratory is maintained in cooperation with the University of Wisconsin.

*Wood and Fiber Science*, 22(2), 1990, pp. 173–192

even on the local level. Not surprisingly, most behavior prediction schemes avoid such complications and use empirical relationships between some easily measured property and the desired behavioral characteristic. The current machine stress-rated (MSR) and common visual grading procedures are examples of applied empirical relationships. The accuracy of these methods is inherently limited by any deficiencies in the relationships they depend on. Closed-form elasticity solutions for the stress field in idealized lumber specimens have been proposed (Green 1945: Tang 1984) but involve too many assumptions and simplifications to be a practical alternative to empirical strength prediction methods. A different approach is required to develop a reliable strength prediction scheme.

Several researchers have recognized the importance of fiber orientation, or grain angle, on structural behavior, and have attempted to use this as the basis for strength prediction schemes. Because of the highly orthotropic nature of wood, a modest angle between the fiber orientation and principal stress direction can have a marked effect on both stiffness and strength. Tests reveal that the tensile strength of a block of clear southern pine with an angle of 12 degrees between the fiber orientation and the applied load has only about half the strength of a similar block with the load applied in line with fibers (Pugel 1986). An implication of this is that the grain deviations that commonly occur around knots and other growth defects affect the structural performance of lumber. Bechtel and Allen developed an empirical procedure that uses measurements of surface grain angles—which describe fiber orientation in the plane of the wide face of a board—to locate a cross section of minimum strength and predict the tensile strength of the board (Bechtel and Allen 1987). This scheme performed well in a preliminary verification and awaits further development. Cramer and others (Cramer and Goodman 1986; Cramer et al. 1988; Cramer and McDonald 1989) have pursued a more theoretical approach and developed a strength prediction scheme that uses surface grain angles as the basis for a finite element model of knot-containing lumber. This model is applied in a step-wise process that simulates the sequence of "local failures" and the resulting accumulation of damage that leads to ultimate failure. This procedure has been used to accurately predict the ultimate tensile strength and effective stiffness of knot-containing 2 by 4 boards and smaller lumber specimens (Cramer and McDonald 1989; Cramer et al. 1988).

While these two strength prediction methods are unique in that they address the grain structure of wood surrounding knots, they are limited to consideration of surface grain angles in the wide-face plane of boards. We will present data that show that the orientation of wood fibers near knots involves *all three* board dimensions. Furthermore, an examination of lumber specimens tested to failure in tension indicates that dive angles—which describe fiber orientation out of the plane of the wide face—can affect the failure process (Badreddine 1988; Anthony and Bodig 1988). If out-of-plane fiber orientations do play a significant role in determining the mode of failure and the strength of lumber specimens subject to tension, they should be considered in new strength prediction methods.

Because of the complex arrangement of fibers near a knot, it is extremely difficult by experimental means to distinguish between the individual effects of surface angle components and dive angle components (in and out of the wide-face plane of a board, respectively). Our approach to this problem has been to enhance the theoretical strength prediction method developed by Cramer and others to in-

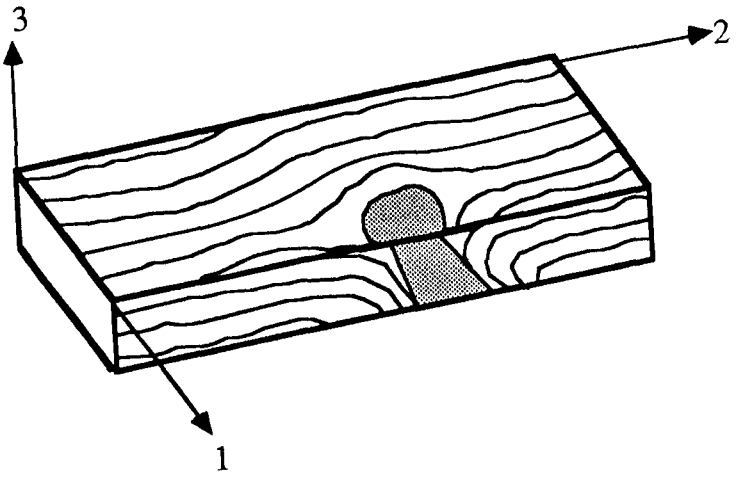


FIG. 1. Surface and dive grain variations shown on board surfaces defined by axes 1, 2, and 3.

corporate consideration of dive angle data. This method has been developed from research contributions from a number of different investigators over the past decade (Dabholkar 1980; Phillips et al. 1981; Cramer and Goodman 1986; Cramer and McDonald 1989, Cramer et al. 1988; Anthony and Bodig 1988; Badreddine 1988; Juedes 1986; Schmidt 1987) and has recently been embodied in the finite element model entitled GASPP (Grain Angle Strength Prediction Program) (Cramer et al. 1988). To distinguish our new contributions from past work, we will refer to the new version of GASPP, which accounts for dive angles, as GASPP+. By comparing strength predictions made with and without the inclusion of dive to the results of physical testing, we have been able to isolate the effect of dive, and to propose when it is and is not of critical importance. In this paper, we will review the strength prediction scheme, present the modifications required to incorporate dive, and present strength predictions and associated experimental results.

### *Description of three-dimensional geometry*

The highly orthotropic nature of structural lumber is a result of the arrangement of fibers in a log. Natural axes in the log are related to the direction of fibers and the orientation of annual rings: "L" signifies "longitudinal," or the direction parallel to fibers. "R" and "T" are "radial" and "tangential" directions relative to the annual rings; both are perpendicular to L. A different coordinate system is used to describe the geometry of a board. Axes 1, 2, and 3 in Fig. 1 are directions relative to the sawn edges of the board. In this defect-containing board, there are significant deviations in fiber orientation near the knot. Lines shown in Fig. 1 on the wide face (1-2 plane) and the edge (2-3 plane) represent the projections of the longitudinal fiber direction in three dimensions onto each plane and should not be confused with annual ring patterns on each surface. We define the angle between the projection of fiber direction onto the 1-2 plane and the 2 axis as the surface grain angle, and the angle between the projection of fiber direction onto the 2-3 plane and the 2 axis as the dive grain angle. Every location in the board has both

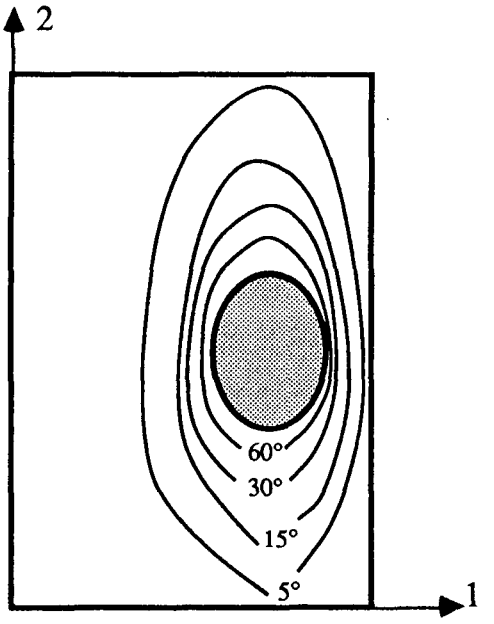


FIG. 2. Typical contours of dive surrounding a knot as established from grain angle scanning.

a surface and a dive angle; both are required to fully describe the orientation in three dimensions of the longitudinal fiber axis with respect to board axes.

Fiber or grain angles can be measured quickly for many discrete points over a board surface with commercially developed grain angle indicators (McLauchlan et al. 1973; McDonald and Bendtsen 1986; Matthews and Soest 1986; Bechtel and Allen 1987). As indicated in the references, at least two different devices exist, each having its own advantages and limitations. To date, neither of these devices gives a complete map of surface and dive angles for all locations on a board, so it is necessary to have general knowledge of dive angles to overcome the shortcomings of each device. A third device under development in Japan shows promise for establishing three-dimensional grain angles, but has been demonstrated on only a small sample of lumber (Sugimori and Sadoh 1988).

Our research has indicated that when dive angles are not or cannot be measured at all locations on a board, a map of dive angles can be simulated. Using the grain angle indicator facility at the University of Wisconsin, we measured dive angle variation in a small set of randomly chosen lumber to establish the approximate region and magnitude of dive angles that can typically be expected to occur near a knot.

Ten knot-containing specimens were chosen from three primarily flat-grained boards: a spruce/pine/fir 2 by 6 (specimens 1, 2, 3, 4), a hem-fir 2 by 8 (specimens 5, 6, 7), and a spruce/pine/fir 2 by 4 (specimens 8, 9, 10). The knots ranged in size from approximately ½-inch to 1-¾-inch average diameter. A series of board edge scans were made on a ¼ by ¼-inch grid over an 8-inch length including the knot. First an edge of the specimen was scanned, then ¼ inch of the edge was removed to expose a new "edge." This new edge was scanned, and another ¼

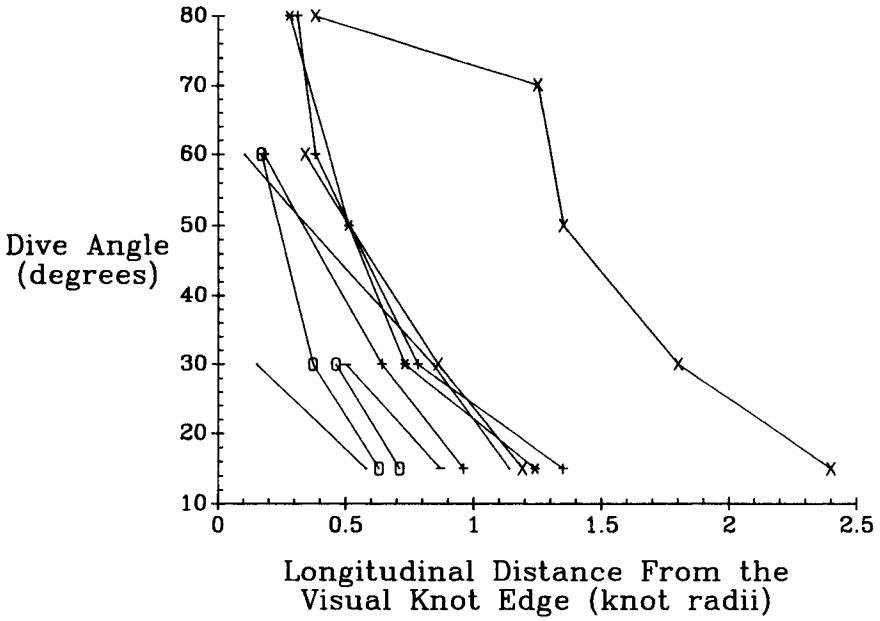


FIG. 3. Measured decline of dive angle as a function of longitudinal distance from the knot edge for 10 specimens studied.

inch was removed, etc. Note that all scans measured surface angles, and that a surface angle on the narrow face (2-3 plane) of the board is a dive angle from the perspective of the wide face (1-2 plane). More specific details of the testing can be found in Stahl (1988).

The maximum dive angle measured for each specimen ranged from 34 to 90 degrees, with seven of the ten maxima above 70 degrees. The maximum values likely would have been consistently close to 90 degrees had all the knot centerlines been oriented normal to the wide face plane and if scanner measurements had always fallen directly outside the knot boundary rather than on the ¼ by ¼-inch grid. Contours of dive around a knot are typically as shown in Fig. 2. Note that the dive contours extend much farther above and below the knot than on each side of the knot. We hypothesized that the decrease in dive angle as one moves away from a knot could be characterized as a function of the average radius of the knot. The typical specimen has a 15 degree dive angle contour, which is an ellipse extending 0.9 radii longitudinally from the knot boundary and 0.2 radii transversely from the boundary. Knot radii refer to the average of the transverse and longitudinal radii of each knot. Figure 3 shows the decline of dive angle as a function of distance from knot edge expressed in terms of knot radii for the 10 specimens studied. Although considerable variability is shown, this small survey indicates that significant dive angles do occur in definable regions near knots.

*Modeling lumber with three-dimensional characteristics in two dimensions*

The three-dimensional orientation of fiber angles near a knot might lead one to believe that a three-dimensional theoretical model of lumber is necessary. As we will discuss here, this is not the case. In the majority of structural lumber

applications, loads are applied and support is provided in such a manner that we can assume that we are dealing with a plane system. Lumber floor joists and members in fabricated trusses are examples of structural elements that are usually designed by considering only forces in one plane of the member. Structural mechanics theory for orthotropic materials reveals, however, that in regions where fiber orientation is not aligned with the plane of loading significant out-of-plane strains are induced. In a board where out-of-plane fiber orientation varies from point to point, these strains are restrained by adjacent material and out-of-plane stresses result. We are not so interested in these strains and stresses themselves, but rather in the effect that these stresses will have on the structural performance of the member. Therefore, we do not believe it is necessary to deal with the out-of-plane direction explicitly, but we have devised a method to account for the out-of-plane fiber orientation in a plane model.

In addition to accommodating diving grain effect, a two-dimensional model must also account for the fact that each wide face of a lumber member may be significantly different than the opposing wide face with respect to grain angles and knot characteristics. A plane parallel to and midway between the two wide faces is called the "mid-surface." We have found that in many cases the mid-surface grain angle maps (surface and dive angles) are adequate representations of the entire three-dimensional board. This is an especially good approximation for flat-grained boards in which the wide face (1-2 plane) corresponds to the L-T plane; it is less accurate for edge-grained boards, where the axes of knots are not approximately perpendicular to the wide face. Grain angle maps for the mid-surface plane are created by averaging the two wide face grain angle measurements after the maps for the faces are shifted to align the knot centers (Juedes 1986; Cramer and McDonald 1989). Henceforth fibers or stresses oriented in the plane of the mid-surface are referred to as "in-plane," with other orientations being "out-of-plane."

Yet another three-dimensional characteristic of lumber concerns the variation of the ring angle at different locations in the cross-section. The ring angle describes the relationship between the R and T fiber directions and board axes. Because the difference in strength or stiffness between the R and T directions is small compared to the difference between either of these directions and the L direction, ignoring the ring angle altogether does not introduce detectable error in our modeling. To avoid confusion, we use the term "transverse" to refer to any direction perpendicular to L.

Given these limitations and simplifications, all we need to completely describe the board's geometry and serve as the basis for a two-dimensional model are the surface and dive grain angle maps generated for the mid-surface. These are used to construct a finite element representation of the board. The map of surface angles is used to define the edges of finite elements, so the "mesh" looks like the projection of fibers onto the surface of the board (see Fig. 4). Lines that follow the longitudinal fiber direction (based on the surface angles) are called "grainlines" and are included as part of the finite element mesh to facilitate the simulation of fracture. The grainlines are deflected by the surface angles around the knot, which is idealized as an ellipse with major and minor axes aligned with the board axes (Juedes 1986). This "mesh generation" is done within the software of the model automatically; the analyst controls the mesh fineness and location of grainlines.

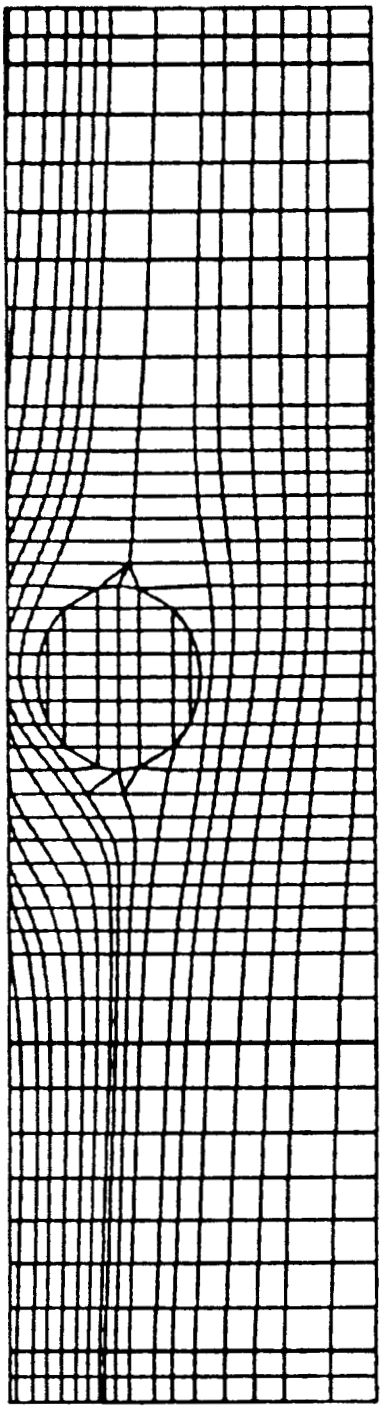

FIG. 4. Typical finite element mesh displaying surface angle variations of a knot-containing board.

Each finite element is assigned a surface and dive angle at its centroid based on the grain angle maps.

Well-established finite element theory states that we can solve for the stresses within the simulated board if we can accurately establish its stiffness. This stiffness is computed as an assembly of the individual element stiffnesses.

Our goal is to formulate a two-dimensional plane stress model which, when subject to uniaxial loading, will have the same stresses and strains as the in-plane stresses and strains of a three-dimensional model. Incorporating the effect of out-of-plane fiber orientation into a two-dimensional model is similar to the problem of including the effect of "secondary" degrees of freedom into a "primary" system without increasing the size of the stiffness matrix. This can be accomplished by an established procedure called static condensation (Cook 1981). We have found it to be more convenient, however, to initially work with the compliance matrix and to later invert it to realize a material stiffness matrix.

First, the untransformed 6 by 6 compliance matrix for a three-dimensional orthotropic material is constructed as in Eq. [1] (Bodig and Jayne 1982):

$$\begin{Bmatrix} \gamma_{11} \\ \gamma_{22} \\ \gamma_{33} \\ \gamma_{12} \\ \gamma_{23} \\ \gamma_{31} \end{Bmatrix} = \begin{bmatrix} \frac{1}{E_1} & \frac{-\upsilon_{12}}{E_1} & \frac{-\upsilon_{13}}{E_1} & 0 & 0 & 0 \\ \frac{-\upsilon_{21}}{E_2} & \frac{1}{E_2} & \frac{-\upsilon_{23}}{E_2} & 0 & 0 & 0 \\ \frac{-\upsilon_{31}}{E_3} & \frac{-\upsilon_{32}}{E_3} & \frac{1}{E_3} & 0 & 0 & 0 \\ 0 & 0 & 0 & \frac{1}{G_{12}} & 0 & 0 \\ 0 & 0 & 0 & 0 & \frac{1}{G_{23}} & 0 \\ 0 & 0 & 0 & 0 & 0 & \frac{1}{G_{31}} \end{bmatrix} \begin{Bmatrix} \sigma_{11} \\ \sigma_{22} \\ \sigma_{33} \\ \tau_{12} \\ \tau_{23} \\ \tau_{31} \end{Bmatrix} \quad [1]$$

where

$\gamma_{ij}$ = engineering strains,
$\sigma_{ij}$ = engineering stresses,
$E_i$ = modulus of elasticity in "i" direction,
$\upsilon_{ij}$ = Poisson's ratio for the "ij" plane,
$G_{ij}$ = shear modulus for the "ij" plane.

This compliance matrix is transformed for both the surface and dive angles in Eq. [2] and results in a full (all terms may be nonzero) 6 by 6 compliance matrix.

$$[S]_{6\times6} = [T_S][T_D][S][T_D{}^{-1}][T_S{}^{-1}] \quad [2]$$

where,

$[S]_{6\times6}$ = the three-dimensional material compliance matrix transformed for surface and dive angles,
$[T_S]$ = the 6 by 6 transformation matrix for surface angle (Stahl 1988; Bodig and Jayne 1982),

$[T_D]$ = the 6 by 6 transformation matrix for dive angle (Stahl 1988; Bodig and Jayne 1982),

$[S]$ = the untransformed material compliance matrix (see Eq. [1]).

As shown in Eq. [3], the coefficients which relate in-plane stresses and strains are simply plucked from this matrix for use in the 3 by 3 compliance matrix for the two-dimensional model.

$$[S]_{3\times3} = \begin{bmatrix} S_{1111} & S_{1122} & S_{1112} \\ S_{2211} & S_{2222} & S_{2212} \\ S_{1211} & S_{1222} & S_{1212} \end{bmatrix} = \begin{bmatrix} S_{1111} & S_{1122} & \cdots & S_{1112} & \cdots & \cdots \\ S_{2211} & S_{2222} & \cdots & S_{2212} & \cdots & \cdots \\ \cdots & \cdots & \cdots & \cdots & \cdots & \cdots \\ S_{1211} & S_{1222} & \cdots & S_{1212} & \cdots & \cdots \\ \cdots & \cdots & \cdots & \cdots & \cdots & \cdots \\ \cdots & \cdots & \cdots & \cdots & \cdots & \cdots \end{bmatrix} \quad [3]$$

where $[S]_{3\times3}$ = the two-dimensional plane stress material compliance matrix transformed for surface and dive angles. Proof of the theoretical validity of this operation for plane stress conditions has been demonstrated by Stahl (1988).

Finally, the resulting 3 by 3 compliance matrix is inverted to get the 3 by 3 material stiffness matrix. This is used to develop the element and board stiffness matrices for the two-dimensional model, which includes the effect of dive (GASPP+). With the stiffness matrix established as presented, displacements and stresses within the wide-face plane are computed in the conventional manner. These displacements and stresses are the key components in our methodology for predicting the structural behavior of lumber specimens.

### *A description of the tensile behavior of knot-containing lumber specimens*

The load-displacement plot of a tension test is a record of the structural response of the lumber specimen up to and including ultimate failure. A typical load-displacement plot from a displacement control test we conducted is shown in Fig. 5. Similar plots have been shown by Anthony and Bodig (1988). Note the drops in the load at several locations in Fig. 5. Previous numerical work and testing we have conducted has given us some insight on what these drops represent; they are the result of instantaneous stiffness loss incurred when parts of the specimen break (Cramer et al. 1988). Such breaks are called "local failures" to distinguish them from the ultimate failure, or collapse, of the specimen. We have previously provided evidence that the ultimate failure of the specimen is the result of a process rather than a single event (Cramer et al. 1988). This "failure process" is the accumulation of damage, in the form of cracks, which result from local failures. A local failure can either result in the initiation of a new crack or the propagation of an existing crack. Each vertical segment on the load-displacement plot may be the result of a single local failure; more likely it is the result of a series of local failures that happen instantaneously. A typical sequence of local failures is a crack initiation followed by propagation of the crack.

Note that between local failures the load-displacement plot (Fig. 5) indicates that the specimen maintains linear behavior. This is almost always the case for tension tests; it results in less complicated modeling.

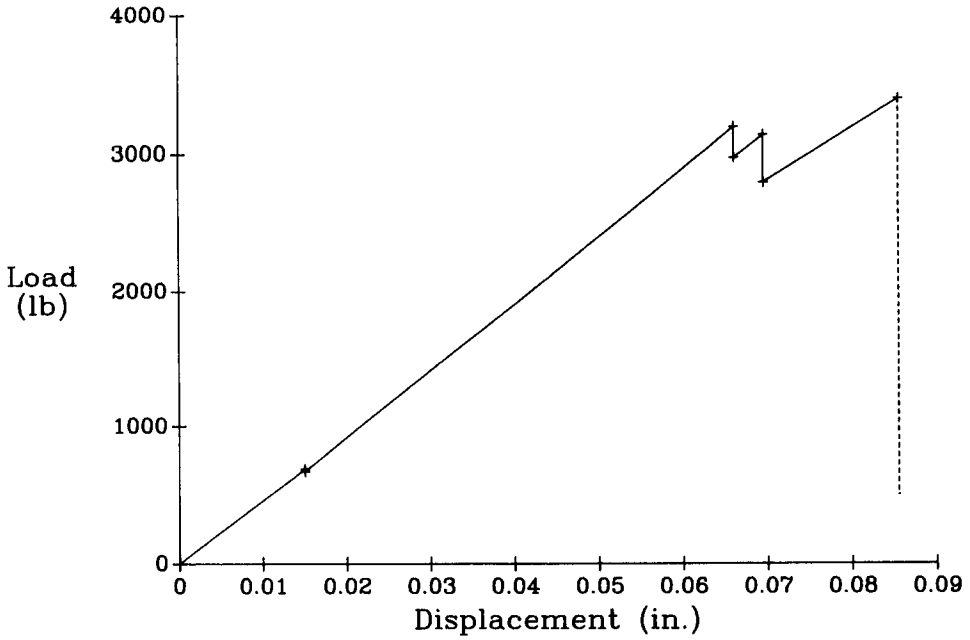


FIG. 5. Typical load-displacement plot from a tension test of a lumber specimen.

We attribute a crack that extends across the grain ("A" in Fig. 6) to fibers breaking and classify it as a tension parallel-to-grain failure. A crack between fibers ("B" in Fig. 6) is attributed to a tension perpendicular-to-grain failure or a shear failure. We have observed that out-of-plane failures sometimes occur when the dive angle is non-zero in a critical location ("C" in Fig. 6). This crack appears on the wide face to be the result of a tension parallel-to-grain failure, but when we consider the edge of the board, we see that the crack is actually the result of a perpendicular-to-grain failure out-of-plane. We address this problem in the GASPP+ model.

### *Simulating the failure process*

The solution of the finite element mesh results in stresses at each element's centroid, displacements along element edges, and stress intensity factors for each crack tip (Cramer and Fohrell 1989). Computed stresses are transformed through the surface angle to give stresses in local coordinates: tension (or compression) parallel ($\sigma\|$) and perpendicular ($\sigma_\perp$) to the projection of true fiber orientation onto the modeling plane, and shear ($\tau$) in this plane. Local failure criteria are required to evaluate the tendency of these stresses to cause crack initiation, and the tendency of stress intensity factors to cause crack tip propagation.

Several local failure theories have been proposed for wood, based on limitations of stress, strain, or energy (Bodig and Jayne 1982). We use the maximum stress theory, which states that each stress should be compared separately to the corresponding strength: stress parallel-to-grain is compared to uniaxial strength parallel-to-grain, shear stress is compared to shear strength, etc. Although intuition may suggest that there should be some interaction between the various compo-

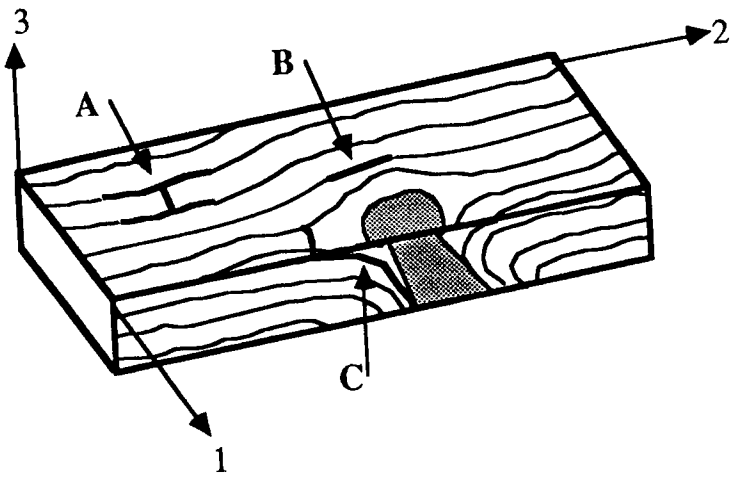


FIG. 6. Idealized cracks in a thin lumber specimen. "A" refers to a crack associated with tension parallel-to-grain failure, "B" refers to a crack associated with tension perpendicular-to-grain or shear failure and "C" refers to a crack associated with failure associated with out-of-plane fiber orientations.

nents, no experimental evidence has been produced to indicate that the maximum stress theory is inadequate or that the more complex theories are superior.

Before applying these criteria, however, we must consider the relationship between the projections of fibers onto the modeling plane (the 1-2 plane) and the orientations of fibers in three dimensions. In three dimensions, there is only one direction that is parallel to the fibers (this is the L direction), but any direction perpendicular to this is truly perpendicular-to-grain. Thus $\sigma_\perp$ in the modeling plane should be compared directly to strength perpendicular-to-grain, $\sigma_\perp$-ult, and $\tau$ can be compared directly to $\tau$-ult, regardless of the magnitude of the dive angle. However, in the presence of a nonzero dive angle $\sigma\|$ in the modeling plane is not actually parallel to the three-dimensional orientation of fibers; it is offset by the dive angle. Consider the element shown in Fig. 7. This element from the model is given a thickness (the dimension in the 3 direction) only to show the non-zero dive angle, represented by light lines on the 2-3 edge. Light lines on the 1-2 plane, or the modeling plane, indicate that this element has a zero surface angle. The stress labelled $\sigma\|$ is the stress in the 1-2 plane, which is parallel to the projection of true fiber direction onto this plane. If we neglect the dive angle, the only failure that $\sigma\|$ could cause is a parallel-to-grain failure, or a breaking of fibers. If, however, we recognize that this element represents a finite volume of wood, and that the dive angle is non-zero, out-of-plane failure modes are possible. By transforming each uniaxial strength through the dive angle, we get three separate criteria for $\sigma\|$ to cause failure of the element:

$$\sigma\| \text{ causes failure at minimum of } \begin{matrix} \dfrac{2\sigma\|_{-\text{ult}}}{1 + \cos(2\theta_D)} \\ \dfrac{2\sigma_{\perp-\text{ult}}}{1 - \cos(2\theta_D)} \\ \dfrac{2\tau_{\text{ult}}}{\sin(2\theta_D)} \end{matrix} \qquad [4]$$

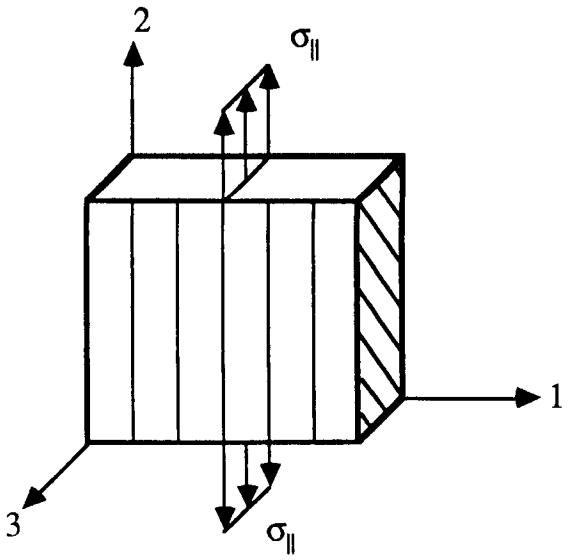


FIG. 7. An element from the GASPP+ model given thickness only to illustrate the nonzero dive angle.

where $\theta_D$ is the dive angle. Note that all three modes will produce a crack that appears on the modeling plane as a crack across grainlines. Thus the local criteria for crack initiation in the GASPP+ model are:

$$\frac{\sigma_{\perp}}{\sigma_{\perp-ult}} = 1, \frac{\tau}{\tau_{ult}} = 1, \frac{\sigma\|}{f} = 1 \quad [5]$$

where f is the minimum of equations [4]. In a model that neglects dive, f is replaced with $\sigma\|$-ult.

Modeling three-dimensional fracture would be a formidable task, as through-thickness cracks would be surfaces instead of lines, and crack tips would be lines instead of points. Certainly our current understanding of wood fracture does not justify the complexities of modeling three-dimensional fracture. Because the two modes of in-plane fracture are related to shear and tension perpendicular-to-grain failures, we assume they are not affected by the dive angle. Wu's fracture criterion (Wu 1967) is used to assess the tendency of cracks to propagate regardless of whether or not dive is considered; this criterion states that a crack tip will propagate when:

$$\frac{K_I}{K_{IC}} + \left(\frac{K_{II}}{K_{IIC}}\right)^2 = 1.0 \quad [6]$$

where $K_I$ and $K_{II}$ are the stress intensity factors for propagation modes I and II, and $K_{IC}$ and $K_{IIC}$ are the corresponding critical values (similar to strengths).

Each element and crack tip is checked for all possible modes of local failure, and the location where any type of failure occurs at the lowest load is identified as the first local failure. Damage is then installed to reflect the different types of local failure previously discussed. A tension perpendicular-to-grain failure or a

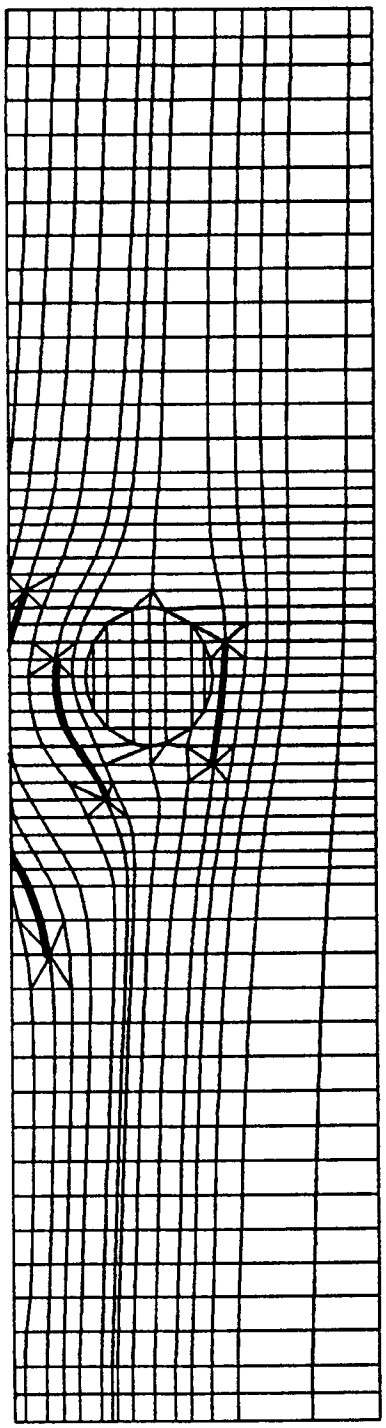

FIG. 8. Typical finite element mesh displaying accumulated fractures as indicated by the bold lines surrounded at each crack tip by eight triangular singular elements.

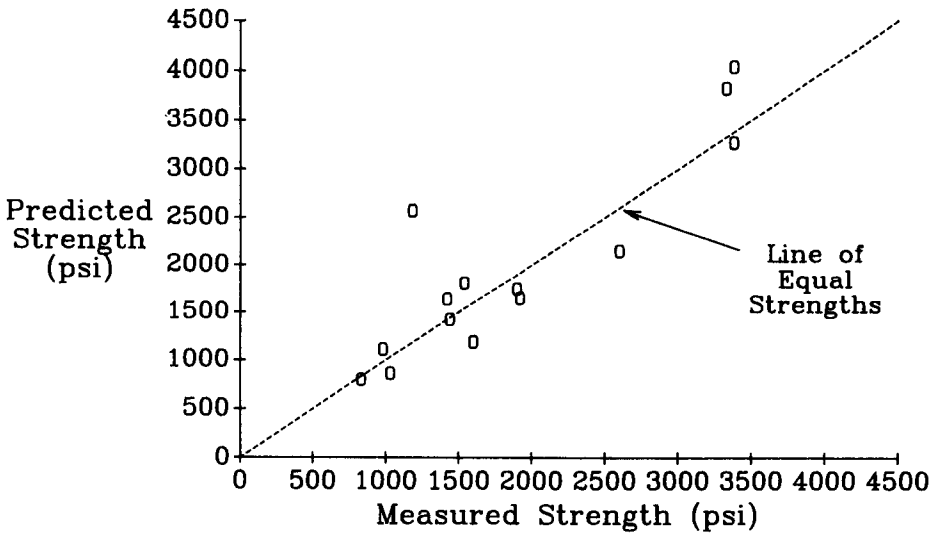


FIG. 9. Predicted GASPP+ board strengths versus measured board strengths.

shear failure is modeled as a longitudinal crack along the grainline between elements. Nodes are added so the elements on either side of the crack are not connected. Singularity elements surround each crack tip (Freese and Tracey 1976); these are used in the fracture mechanics calculations (Cramer and Fohrell 1989). A tension parallel-to-grain failure is modeled as a transverse crack adjacent to the failed element with longitudinal cracks at each end of the transverse crack. This represents the real tendency of wood to splinter rather than crack in long straight lines across grain. If the specified first failure is the propagation of an existing crack, the analyst adds damage by making the crack longer by an amount of one or two finite element lengths. The modified model is reanalyzed, the next local failure is identified, and additional damage is installed. Figure 8 shows a model where several cracks have accumulated prior to reaching maximum load. The cracks are indicated by the bold lines surrounded at each crack tip by 8 triangular singular elements.

The raw results of a complete GASPP+ analysis are values for board flexibility and for the applied stress causing local failure of each "sub-model." Board flexibility always increases from one run to the next, as damage has been added at the end of the previous run. Applied stress to cause local failure may change dramatically from one run to the next as, for instance, a crack may be initiated at a certain load but then the same crack may propagate at a much lower load. Finally the load-displacement record is plotted and the maximum load attained is called the ultimate strength.

### *Application and verification of the two-dimensional model with dive considerations (GASPP+)*

Specimens used in this study phase were prepared and donated by the Weyerhaeuser Company. Mill-run southern pine 2 by 4s were selected to contain a single or double knot near the center of an otherwise clear five foot length. Each

TABLE 1. *Measured, GASPP predicted, and GASPP+ predicted ultimate loads.*

| Specimen number | Knot type | Test value (lb) | GASPP strength (lb) | Error (%) | GASPP+ strength (lb) | Error (%) |
|---|---|---|---|---|---|---|
| 22 | c | 3,380 | 3,960 | 17 | 4,042 | 20 |
| 43 | c | 1,420 | 2,575 | 81 | 1,640 | 15 |
| 81 | e | 1,600 | 1,362 | −15 | 1,189 | −26 |
| 101 | e | 830 | 1,265 | 52 | 798 | −4 |
| 102 | c | 1,900 | 2,147 | 13 | 1,748 | −8 |
| 103 | c | 3,380 | 3,769 | 12 | 3,270 | −3 |
| 113 | c | 1,184 | 3,685 | 211 | 2,571 | 117 |
| 173 | e | 1,030 | 2,053 | 99 | 863 | −16 |
| 32 | c | 1,440 | | | 1,422 | −1 |
| 73 | e | 980 | | | 1,110 | 13 |
| 82 | e | 1,540 | | | 1,813 | 18 |
| 132 | c | 1,920 | | | 1,648 | −14 |
| 142 | c | 2,600 | | | 2,147 | −17 |
| 151 | c | 3,330 | | | 3,822 | 15 |
| Correlation coeff., r | | | 0.69 | | 0.89 | |
| Ave. absolute error | | | 62% | | 21% | |

* Knot type codes as defined by ASTM D245: "c" = center knot, "e" = edge knot.

2 by 4 was then sliced parallel to the wide face to produce three 3.5 by 0.25 by 60-inch specimens. Both wide faces of each of the specimens were scanned for local grain angle at the Weyerhaeuser Technology Center using Weyerhaeuser's optical scanner; this scanner gives grain angle maps for both surface and dive angles. A grid 3 mm by 3 mm was used for the grain angle map; the entire width of the specimen's face and a length extending well above and below the defect(s) was scanned. At the University of Wisconsin Structures and Materials Laboratory, a 40-inch defect-containing portion of each of the specimens was tested to failure in tension. An MTS 810 testing machine was used with friction grips, which were specially designed to reduce stress concentrations and to allow the ends of the specimens to rotate freely. A displacement control rate of 0.0125 inches per minute was used; most tests lasted approximately ten minutes (Badreddine 1988).

Clearwood and knotwood properties needed for GASPP+ analysis are those required for Eqs. [1], [4] and [6] and were either measured or predicted using established relationships (Badreddine 1988; Bodig and Goodman 1973; Pugel 1986; Petterson and Bodig 1983; Pugel 1980; Schmidt 1987; Stahl 1988).

Fourteen randomly chosen specimens were analyzed with the GASPP+ model. The number used to identify each specimen reflects the specimen's preparation: specimen 22 is slice No. 2 from 2 by 4 No. 2; specimen 151 is slice No. 1 from 2 by 4 No. 15; etc. Each analysis consisted of between 20 and 45 failure modeling steps in the step-wise simulation process.

Ultimate load predictions made with the GASPP+ model are shown in Table 1 and Fig. 9. The average error is 21%, and the correlation coefficient is 0.89. Approximately equal numbers of strengths are over- and under-predicted. Twelve of fourteen specimens have absolute errors under 20%. Errors do not appear to be related to knot location.

In order to see the effect of dive on these results, eight of the specimens were analyzed using surface grain angles only. When these eight strength predictions

TABLE 2. *Measured, ASTM D245 predicted, and GASPP+ predicted ultimate loads.*

| Specimen number | Knot type | Test value (lb) | ASTM D245 strength (lb) | Error (%) | GASPP+ strength (lb) | Error (%) |
|---|---|---|---|---|---|---|
| 22 | c | 3,380 | 3,690 | 9 | 4,042 | 20 |
| 43 | c | 1,420 | 3,190 | 125 | 1,640 | 15 |
| 81 | e | 1,600 | 2,130 | 33 | 1,189 | −26 |
| 101 | e | 830 | 1,810 | 118 | 798 | −4 |
| 102 | c | 1,900 | 3,790 | 99 | 1,748 | −8 |
| 103 | c | 3,380 | 4,010 | 19 | 3,270 | −3 |
| 113 | c | 1,184 | 3,260 | 175 | 2,571 | 117 |
| 173 | e | 1,030 | 1,770 | 72 | 863 | −16 |
| 32 | c | 1,440 | 4,230 | 194 | 1,422 | −1 |
| 73 | e | 980 | 3,540 | 261 | 1,110 | 13 |
| 82 | e | 1,540 | 1,860 | 21 | 1,813 | 18 |
| 132 | c | 1,920 | 3,574 | 86 | 1,648 | −14 |
| 142 | c | 2,600 | 4,800 | 85 | 2,147 | −17 |
| 151 | c | 3,330 | 4,760 | 43 | 3,822 | 15 |
| Correlation coeff., r | | | 0.64 | | 0.89 | |
| Ave. absolute error | | | 95% | | 21% | |

* Knot type codes as defined by ASTM D245: "c" = center knot, "e" = edge knot.

are compared to measured strengths (see Table 1), the average error is 62% and the correlation coefficient is 0.69. This indicates that for this set of specimens, the inclusion of dive is critical in obtaining accurate strength predictions. Furthermore, of specimens analyzed both ways, those with the largest error when dive is neglected show the greatest improvement when dive is included.

When we consider the results of the ASTM strength prediction procedure (ASTM D245 1983) the accuracy of the GASPP+ predictions can be fully appreciated (see Table 2). The high average absolute error in ASTM predictions (95%) is partially due to the significant end rotations experienced by the 40-inch specimens in this study; the ASTM procedure is based on tests of longer specimens, which would not rotate as much as shorter ones. Most of the error, however, is likely due to the crudeness of the scheme, which is the basis for visual lumber grading.

Predicted load-displacement plots were constructed for each specimen and compared to the experimental plots recorded by the MTS testing machine. Load-displacement plots for two of the fourteen specimens analyzed are shown in Fig. 10. These two were chosen to represent the wide range of behavior of defect-containing tensile members, and the ability of the GASPP+ model to predict the very different types of behavior. Note that extra small jumps in the predicted record may be the result of a predicted strength property being just slightly too low; likewise missing small jumps can be the result of a property being slightly high. The load causing first local failure in specimen 43 is the ultimate load; there is no "reserve" strength in the board after first failure. Specimen 82, on the other hand, experiences significant local failures before realizing its ultimate load and retains a substantial amount of strength even after its ultimate load has caused a significant local failure. Photographs showing fracture patterns of the specimens after tensile failure compared favorably to figures of the finite element models at the end of GASPP+ analysis. The crack patterns were similar, indicating that the model does simulate the true behavior of the boards.

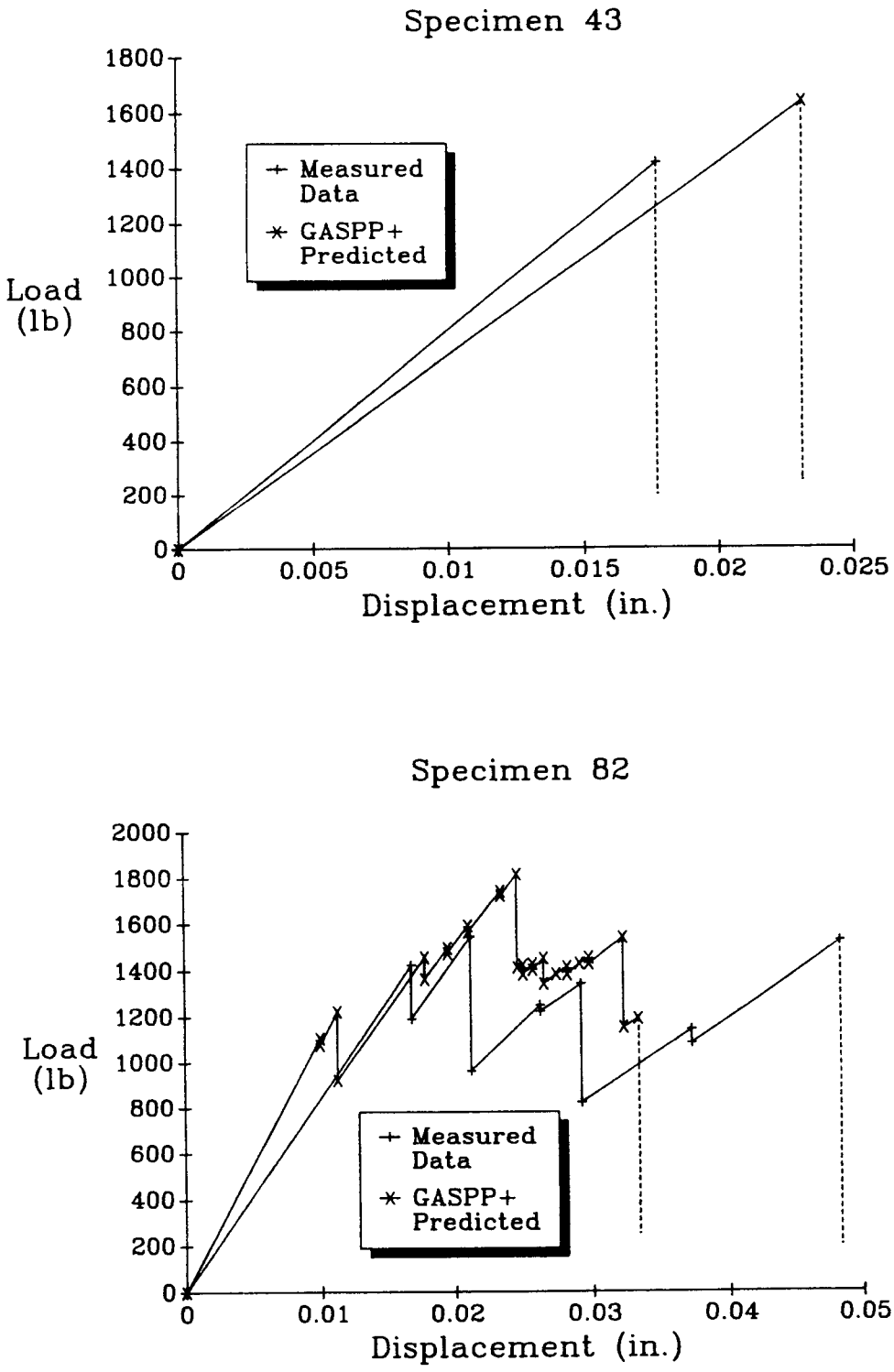


FIG. 10. Failure (load-displacement) records for specimens 43 and 82.

When interpreting these results, we must also consider another study in which the GASPP model, neglecting dive and using surface grain angles only, gave accurate predictions of 2 by 4 tensile strength. Cramer and McDonald (1989) used the original GASPP model to predict the ultimate tensile strength of defect-containing southern pine and Douglas fir 2 by 4s with an average absolute error of 12% and correlation coefficient of 0.86. These results are arguably just as good as the GASPP+ results presented here, and substantially better than the results of the analyses that neglected dive discussed above. The explanation for the seemingly inconsistent results sheds further light on the effect of dive on tensile strength. The differences between the experimental setups and boundary conditions of the Cramer and McDonald study and this study indicate that the importance of the effects of dive angles depends on specimen size and test conditions. In the Cramer and McDonald study, full-thickness 2 by 4 specimens were tested with end rotations restricted, where as here 0.25-inch-thick specimens were tested with specimen ends free to rotate. Observations indicate that the two effects are separate but additive: dive angles influence the failure modes of thin specimens more than thick specimens, and the effect of dive is amplified when specimen ends are permitted to rotate.

From observations gathered in this testing program and two others (Cramer and McDonald 1989; Anthony and Bodig 1988) we believe that different tension testing procedures for lumber specimens will often result in different failure modes and different strengths for otherwise identical specimens. It can be debated which testing procedure most realistically represents the conditions a member will be subject to in use. Unlike empirical methods, the theoretical model contained in GASPP+ can account for different specimen size and testing conditions.

## SUMMARY AND CONCLUSIONS

This paper describes a theoretical model (GASPP+) for predicting the strength and simulating the fracture of lumber specimens. The unique aspect of this two-dimensional model is its ability to account for the three-dimensional orientation of wood fibers near knots in flat-grained boards.

Evidence is provided that shows that grain angles dive from 15 to 90 degrees out of the wide face plane of lumber in a region within about one knot radius from the visual edge of a knot. The diving nature of the grain angles is accounted for in a two-dimensional model, called GASPP+, by transforming a three-dimensional material compliance matrix, and extracting the appropriate coefficients for use in a two-dimensional compliance matrix. Failure criteria are modified to reflect the decreased strength that goes along with nonzero dive angles. These modifications led to accurate tensile behavior predictions, as evidenced by load-displacement plots and ultimate load measurements of lumber specimens.

Application of the GASPP+ model has shown that consideration of dive can be important in predicting the strength and failure mode of thin lumber specimens. When dive angles were considered, GASPP+ strength predictions of thin lumber specimens correlated with measured strengths by a correlation factor of 0.89 and when dive angles were neglected the correlation coefficient dropped to 0.69. On the basis of previous research, we believe that lumber specimen thickness and the manner of loading may influence the magnitude of the dive effect on strength. It is hoped that by continuing this research we will gain a more complete under-

standing of lumber failure and gain the insight needed to develop simpler strength prediction schemes for practical grading applications.

ACKNOWLEDGEMENTS

Dr. Gary Schajer and Dr. William Fohrell, research engineers at the Weyerhaeuser Technology Center in Tacoma, WA have participated in various aspects of this work. Their contributions including providing the lumber specimens and associated grain angle scanning are gratefully acknowledged. This work was made possible by the financial support of the Graduate School of the University of Wisconsin and the Forest Products Laboratory.

REFERENCES

AMERICAN SOCIETY FOR TESTING AND MATERIALS. 1983. Standard methods for establishing structural grades and allowable properties for structural lumber. ASTM Designation: D245-81.

ANTHONY, R., AND J. BODIG. 1988. Tension behavior of knot-containing Douglas-fir boards. Proceedings of the 1988 International Conference on Timber Engineering, vol. 2. Forest Products Research Society. Pp. 779–786.

BADREDDINE, L. 1988. Supporting studies and tests for modeling lumber in tension. M.S. Independent Study Report, Dept. of Civil and Environmental Engineering, University of Wisconsin–Madison.

BECHTEL, F. K., AND J. R. ALLEN. 1987. Methods of implementing grain angle measurements in the machine stress rating process. Proceedings of the Sixth Symposium on Nondestructive Testing of Wood. Washington State University. Pp. 303–353.

BODIG, J., AND J. R. GOODMAN. 1973. Prediction of elastic parameters for wood. Wood Science 5(4): 249–264.

———, AND B. A. JAYNE. 1982. Mechanics of wood and wood composites. Van Nostrand Reinhold Company, Inc., New York.

COOK, R. D. 1981. Concepts and applications of finite element analysis. Second Edition. John Wiley and Sons, Inc., New York.

CRAMER, S. M., AND W. FOHRELL. 1989. Method for simulating the tension performance of lumber members. Proceedings of the Symposium on the Mechanics of Cellulosic and Polymeric Materials, The Third Joint ASCE/ASME Mechanics Conference. Pp. 193–200.

———, AND J. R. GOODMAN. 1986. Failure modeling: A basis for the strength prediction of lumber. Wood Fiber Sci. 18(3):446–459.

———, AND K. MCDONALD. 1989. Predicting lumber tensile stiffness and strength with local grain angle measurements and failure analysis. Wood Fiber Sci. 21(4):393–410.

———, D. C. STAHL, W. B. FOHRELL, AND K. A. MCDONALD. 1988. Exploring the relationship between local grain angle and initial fracture in lumber subject to tensile load. Proceedings of the 1988 International Conference on Timber Engineering, vol. 2. Forest Products Research Society. Pp. 566–575.

DABHOLKAR, A. 1980. Analysis of wood with knots and cross grain. Ph.D. dissertation, Dept. of Civil Engineering. Colorado State University, Ft. Collins.

FREESE, C. E., AND D. M. TRACEY. 1976. The natural isoparametric triangle versus collapsed quadrilateral for elastic crack analysis. Int. J. Fracture 12:767–770.

GREEN, A. E. 1945. Stress systems in aeolotropic plates. Proceedings of the Royal Society of London. PRSLA 184A.

JUEDES, B. M. 1986. Failure modeling of wood tensile members. M.S. Independent Study Report. Dept. of Civil and Environmental Engineering. University of Wisconsin–Madison.

MATTHEWS, P. C., AND J. F. SOEST. 1986. Method for determining localized fiber angle in a three-dimensional fibrous material. U.S. Patent 4,606,345.

MCDONALD, K. A., AND B. A. BENDTSEN. 1986. Measuring localized slope of grain by electrical capacitance. Forest Prod. J. 23(5):75–78.

MCLAUCHLAN, T. A., J. A. NORTON, AND D. J. KUSEC. 1973. Slope-of-grain indicator. Forest Prod. J. 23(5):50–55.

PETTERSON, R. W., AND J. BODIG. 1983. Prediction of the fracture toughness of conifers. Wood Fiber Sci. 15(4):302–316.

PHILLIPS, G. E., J. BODIG, AND J. R. GOODMAN. 1981. Flow-grain analogy. Wood Fiber Sci. 14(2): 55–64.

PUGEL, A. 1980. Evaluation of selected mechanical properties of coniferous knotwood. M.S. thesis, Dept. of Forest and Wood Sciences, Colorado State University, Ft. Collins.

———. 1986. Fracture mechanics-based failure criterion for wood. Ph.D. dissertation, Dept. of Forest and Wood Sciences, Colorado State University, Ft. Collins.

SCHMIDT, M. K. 1987. Modeling considerations for predicting the tensile behavior of lumber. M.S. Independent Study Report. Department of Civil and Environmental Engineering. University of Wisconsin–Madison.

STAHL, D. C. 1988. The effect of "dive" on the tensile behavior of defect containing lumber: Modifications to the U. W. Grain Angle Strength Prediction Program. M.S. thesis, Dept. of Civil and Environmental Engineering, University of Wisconsin–Madison.

SUGIMORI, M., AND T. SADOH. 1988. Measuring three-dimensional grain angles surrounding knots by image processing. J. Japan Wood Research Society 34(8):647–651.

TANG, R. C. 1984. Stress concentration around knots in laminated beams. Wood Fiber Sci. 16(1): 57–71.

WU, E. M. 1967. Application of fracture mechanics to orthotropic plates. J. Appl. Mech. 12:967–974.